NASA Technical Memorandum 85953

Airborne Astronomy Program
Medium Altitude Missions Branch
Preprint Series 012

NASA-TM-85953 19840018457

The Energetics and Mass Structure of Regions of Star Formation: S201

Harley A. Thronson, Jr.,
Howard A. Smith, Charles J. Lada,
W. Glaccum, D.A Harper,
R.F Loewenstein, and
J. Smith.

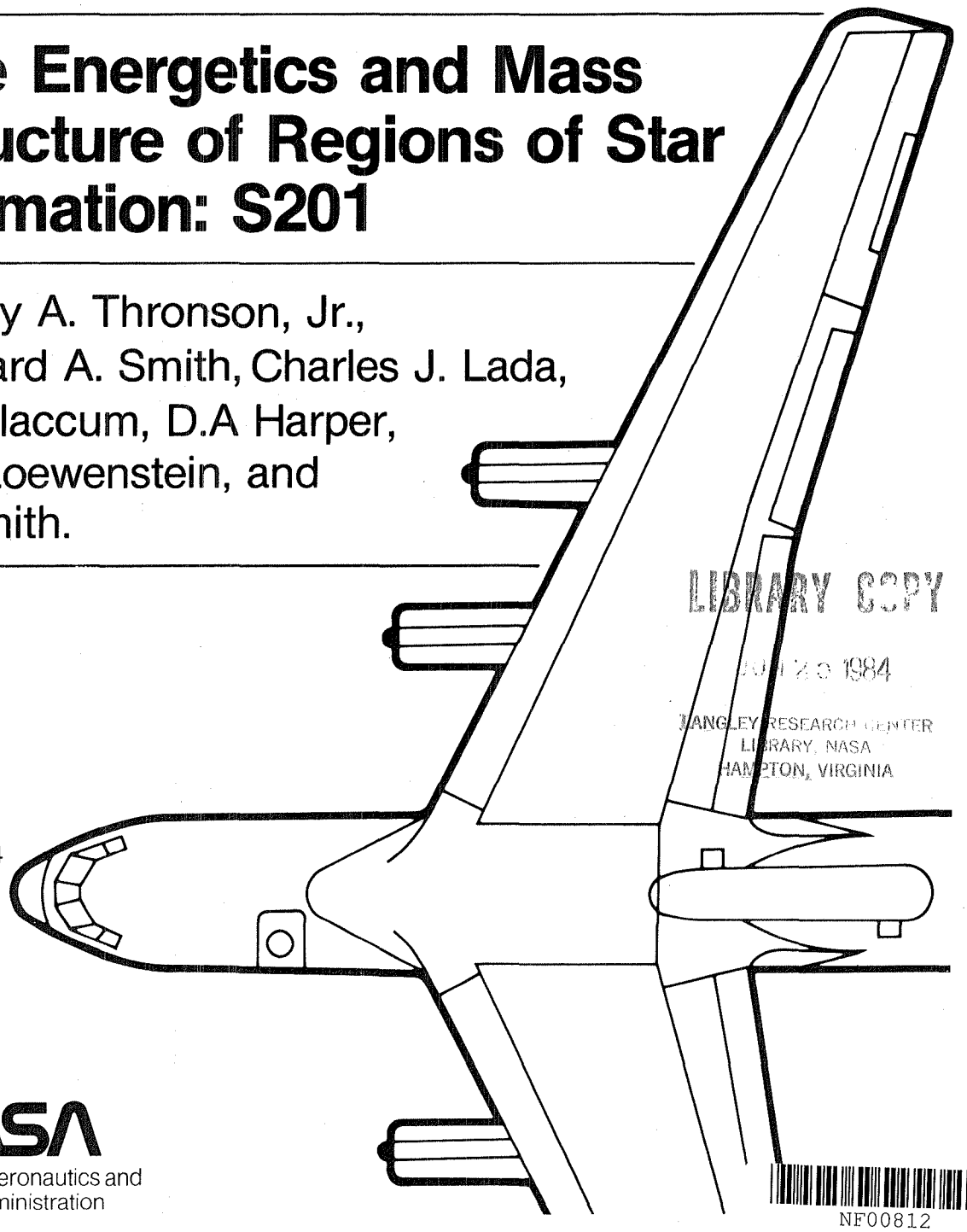

May 1984

NASA
National Aeronautics and
Space Administration

NASA Technical Memorandum 85953

Airborne Astronomy Program
Medium Altitude Missions Branch
Preprint Series 012

The Energetics and Mass Structure of Regions of Star Formation: S201

Harley A. Thronson, Jr., University of Wyoming, Laramie, Wyoming
Howard A. Smith, Naval Research Laboratory, Washington, D. C.
Charles J. Lada, University of Arizona, Tucson, Arizona
W. Glaccum
D. A. Harper
R. F. Loewenstein
J. Smith, Yerkes Observatory, Williams Bay, Wisconsin

National Aeronautics and
Space Administration

Ames Research Center
Moffett Field, California 94035

MNRAS, in press

THE ENERGETICS AND MASS STRUCTURE OF REGIONS OF STAR FORMATION: S201

Harley A. Thronson, Jr.
Wyoming Infrared Observatory
University of Wyoming
Laramie, Wyoming 82071 USA

Howard A. Smith
E. O. Hulbert Center for Space Research
Naval Research Laboratory
Washington, D.C. 20375 USA

Charles J. Lada[1]
Steward Observatory
University of Arizona
Tucson, Arizona 85721 USA

and

W. Glaccum, D. A. Harper, R. F. Loewenstein, and J. Smith
Yerkes Observatory
Williams Bay, Wisconsin 53191 USA

Received: _____

[1]Alfred Sloan Foundation Fellow

I. INTRODUCTION

The interaction between the molecular component of a star-forming cloud and the dust component is one of the most important in astrophysics. The gas temperature is important in determining the mass of stars yet to form, the small-scale thermal motions of the clouds, and some molecular reactions. The dust plays the role of regulator in the energy flow from a new star to the surrounding gas. If the molecules and grains are collisionally coupled, both can be easily heated by the luminous objects forming within the cloud.

The theoretical understanding of these processes is reasonably advanced. Consequently, it is important to obtain suitable detailed observations of the dust for direct comparison with, primarily, radio molecular and continuum data. Broad-band far-infrared photometry and mapping is the most effective method for studying the temperature and mass structure of grains in the star-forming clouds. For this reason we have been carrying out a series of infrared/radio observations of a collection of young objects in order to effectively study the role of dust in molecular clouds. This study has included dark clouds (Lada et al. 1981), remnant material surrounding young stars (Smith et al. 1982), the final disruption of clouds surrounding very energetic stars (Thronson et al. 1982), and the effects of winds on molecular clouds (Schwartz et al. 1983). In this paper we report on a fourth type of object: an extensive infrared/molecular cloud still surrounding a moderately-luminous star. The object is S201. It was chosen because the density is low enough so that not all the stellar radiation is absorbed close to the star, yet is high enough to allow some thermal coupling between the dust and gas. The infrared emission should

ABSTRACT

A number of theoretical predictions about dust and gas in star-forming regions are tested by observing a 4' region surrounding the radio continuum source in S201. The object was mapped in two far-infrared wavelengths and was found to show significant extended emission. Under the assumption that the molecular gas is heated solely via thermal coupling with the dust, the volume density was mapped in S201. The ratio of infrared optical depth to CO column density was calculated for a number of positions in the source. Near the center of the cloud our values are found to be in good agreement with other determinations for lower column density regions. In addition, our observations suggest significant molecular destruction in the outer parts of the object. Current models of gas heating were used to calculate a strong limit for the radius of the far-infrared-emitting grains, $a \leq 0.15$ μm. In addition, we argue that grains of about this size are required by the observation of high-temperature ($T \geq 20$ K) gas in many sources.

therefore be extensive, which allows a direct comparison between the dust and the gas emission over a fairly wide area of sky and presumably over a wide range of physical conditions.

S201 is also in one of the most interesting parts of the sky. It is apparently the easternmost member of the string of H II regions dominated by the giants W3, W4, and W5. S201 has been mapped at high angular resolution in the radio continuum by Felli and Hjellming (1982, in preparation) and in the J = 1→0 line of ^{12}CO and ^{13}CO (Martin and Barrett 1978). The source AFGL 416 is centered on the optical nebula, and Kleinmann et al. (1979) found a small-scale local maximum at the position of the radio continuum peak within the extended 10.6 μm emission. At lower resolution the region was mapped in CO by Lada et al (1978), in the radio continuum by Vallée, Hughes, and Viner (1979), and in the mid-infrared by Thronson and Price (1982). In all cases S201 appears as a distinct, often quite bright, object. Visually the object appears about to break up — or break through — surrounding neutral material.

II. OBSERVATIONS AND REDUCTIONS

a) The Far-infrared

The extended far-infrared emission from S201 was observed during January, 1981 using the 0.9 m telescope onboard NASA's Kuiper Airborne Observatory. Two detector systems were used. One was a multi-filter 7-channel array, each channel having an angular resolution of 49". This system was used to map the extended emission around the source and to obtain multi-filter observations at a number of positions. The second system was a long wavelength, single-channel detector with an angular resolution of 128". Both systems used liquid-He-cooled bolometers as the detecting element and broad-band filters to define passbands. An east-west chopper throw of 5!7 was used for all observations.

A square approximately 4' on a side (equivalent to 2.7 pc at a distance to S201 of 2.3 kpc [Georgelin and Georgelin 1976]) was mapped in primarily two passbands using the 7-channel system. One filter had half-power points of 45 and 80 μ m and the other was a long-wavelength pass filter that had its 50% cut-on at 85 μ m and an effective wavelength of about 118 μ m. The maps obtained with these filters are shown in Fig. 1. Most of the area shown in the figures was mapped at one-half or one beamwidth resolution. In addition to these maps, the flux at the peak position was measured in a number of filters and the result is presented in Fig. 2. Observed and derived parameters are presented in Table I.

The use of broad filters is effective in allowing low brightness areas to be mapped rapidly. However, converting the measured flux into flux density — a more useful quantity — is not completely straightforward. We have used a standard iterative procedure in which an educated guess is used to find an intrinsic source spectrum. This is

convolved with the filter/detector responses, compared with the observed fluxes, and followed by changes to the original choice of source spectrum. This method allows a determination of effective wavelength for each filter, along with the flux density. The calibration for these observations used Saturn, following Loewenstein et al. (private communication).

As with many galactic far-infrared sources, the derived peak spectrum had a shape much like νB_ν (T): optically-thin emission from an isothermal blackbody multiplied by an absorption efficiency that varies as $Q \propto \nu$. The agreement between it and the actual observations presented here is due partly to the fact that "optically-thin" and "iso-thermal" are often good first approximations to an actual infrared source (e.g., Leung 1976; Scoville and Kwan 1976; Rowan-Robinson 1980), particularly at longer wavelengths. Except for the peak and six points immediately surrounding it, fluxes in only two filters were obtained for positions in the maps (Fig. 1). To estimate dust temperatures for these latter points, we assumed the functional form νB_ν (T), and took T as the dust temperatures, T_d. Fig. 2 shows how well this function fits to at least one position (the peak), where more than two spectral points are available. The internal uncertainties in the flux determinations typically lead to ± 2 K uncertainties in T_d. We believe the total 1σ uncertainty in temperature to be ± 5 K, due primarily to adopting a simple, single analytic function.

As will be discussed in the following section, it was found that there were only relatively small variations in T_d through the source. This is expected behavior for the dust, whose temperature depends very weakly upon all the parameters of significance. As a result, the

spectral shape in the far-infrared changed very little with position, and therefore the calculated mean wavelength for any of the broadband filters was approximately the same at all positions. At no point were there variations greater than 10% from the values shown in the legend to Fig. 1.

With a dust temperature found, the far-infrared emission optical depth was estimated via $F_\nu = \tau B_\nu(T_d)\Omega$, where τ is the optical depth and Ω is the beam solid angle. The 85 μm → ∞ filter (with a nominal effective wavelength of 118 μm) was used to find τ. The uncertainty of ± 5 K estimated in T_d translated to about a ± 50% change in τ_{118}. The optical depths are presented in Fig. 3.

From the spectrum the total luminosity of the object can be estimated. Integrating under the curve in Fig. 2 we find $L = 1.3 \pm 0.3 \times 10^4 L_\odot$ (40-250 μm) at the peak in a 49" beam. The uncertainty is our estimate for the range of spectra allowed by our points. For the area mapped in Fig. 1, $L = 5.7 \pm 1.3 \times 10^4 L_\odot$ at 2.3 kpc over the same wavelength range. This is close to the luminosity of an O9 ZAMS star, the same conclusion as that reached by calculating the type of star required to ionize the H II region observed at radio continuum wavelengths (Vallée, Hughes, and Viner 1979). This calculation of the far-infrared luminosity may be an underestimate of the total luminosity of the source, but probably not by a large factor. Large-beam mid-infrared observations of the region (Thronson and Price 1982) find emission at 11 and 20 μm of only a few tens of Janskys. Although there are not yet any large-scale far-infrared maps of the region, Fig. 1 shows a clean fall-off in all directions from the peak so there is unlikely to be significant emission beyond that which we have mapped.

b) The Mid-infrared

The probable location of the exciting star(s) in the source was searched at 10 μm. Approximately a 1' x 1' box centered on the Kleinmann et al. (1979) mid-infrared position was mapped using the Wyoming Infrared Observatory (WIRO) 2.3 m telescope. A 6.6" aperture with a 30" north-south throw was used to find a limit any point-like source in this area to less than about 1 Jy. The Kleinmann et al. position for the 10 μm source that they found was virtually the same as the location of peak radio continuum flux found by Felli and Hjellming (1982, in preparation). We therefore centered our beam at this position and obtained the flux densities presented in Table I. The system and filter parameters, and the absolute calibration are the same as in Gehrz, Hackwell, and Jones (1974). The quoted uncertainties are internal only; the systematic uncertainties are probably ± 10%. At the same position, Kleinmann et al. found F_ν = 10 Jy at 10.6 μm in a 15" beam. Comparison with our result supports our assumption that the location we observed was that of the exciting star(s) and that it was the peak of an extended distribution of low-surface-brightness mid-infrared emission.

As will be described in § IIIc, the source probably has only a modest amount of dust extinction associated with it: perhaps $A_V \approx 9$ mags at the location of the radio continuum source. The exciting star should therefore suffer very little extinction at 2.3 μm. However this wavelength can show some thermal emission due to hot dust. At the distance of 2.3 kpc, an unextinguished O9 ZAMS star should have $m_{2.3}$ = 14 mags. This is about an order of magnitude fainter than the value in Table I, although of course there is a large uncertainty quoted for our short wavelength data. The 10 μm and 19.5 μm flux densities must be excess emission due to hot dust surrounding the star.

III. DISCUSSION AND ANALYSIS

a) General Source Description

S201 itself is, of course, the visual component to the source. Photographs of the giant W5 H II region show S201 clearly (e.g. Lada et al. 1978; Vallée, Hughes, and Viner 1979; Thronson and Price 1982). It is a bright but broken emission nebula, about 4'.5 across, embedded within an extensive molecular cloud that also encloses at least the eastern part of W5, about 12' to the the west (Thronson and Lada 1983, in preparation). The radio continuum emission peaks near the center of the visible object. The far-infrared maximum appears coincident with the radio continuum peak.

Figure 1 shows a region of extended infrared emission with a half-power width not much larger than our beam size, if that much. However, as is often the case, the lower contours are much more extended. From the limited number of points in the maps, it appears that the infrared emission is rather elongated in the east-west direction, with a local maximum about 2' west of the main peak. The east-west extent is probably greater than that north-south, similar to the maps of 115 GHz CO emission (Martin and Barret 1978). The far-infrared emission drops rapidly about 1½' east of the peak. We believe this to be largely real. However, at this position the infrared reference beam was close to a CO hotspot, and some contamination from associated dust emission may have occurred. It is worth noting that although S201 itself, and the infrared source we are observing, lie at a CO column density maximum, the peak molecular temperature is actually almost 4' further west. Our observations did not extend fully to this point, and it would be a useful position for future investigations.

This east-west elongation becomes even more pronounced in the ^{13}CO column density (Martin and Barrett) and the far-infrared emission optical depth (Fig. 3). The association between these two parameters is the subject of §IIIc.

It is not surprising that the total luminosity of the exciting star(s) as determined from radio continuum observations agrees with that from the infrared data. Only a few magnitudes of dust obscuration is sufficient to absorb virtually all the stellar and nebular uv photons, converting them into the infrared. In the case of S201, the infrared emission is quite extended, suggesting that while the dust <u>is</u> effective in photon absorption, the absorption is in a rather diffuse medium. There would therefore be little dust absorption <u>within</u> the H II region. This lack of competition for Lyman continuum photons between the gas and grains explains why the radio continuum observations should give a good estimate of the luminosity of the exciting stars.

b) <u>Temperature Distribution</u>

Dust temperature variations are quite gentle throughout the area mapped, nowhere varying more than 30% of the maximum. Within the uncertainties, T_d drops off uniformly from 42 K at the peak. Two arcminutes away (excepting to the east), we calculate $T_d = 36 - 38$ K, and at three arcminutes we find $T_d = 30 - 35$ K.

The CO temperatures reported by Martin and Barrett generally show a somewhat similar behavior, but not without interesting exceptions. For the region mapped in the far-infrared, the peak gas and dust temperatures are coincident, with $T_d \approx 2T_g$. However, only 1 arcminute north, the gas temperature has dropped to where $T_d \approx 4\ T_g$, with $T_d \approx 5\ T_g$ two arcminutes north of the maximum. South of the source is rather

similar. The west side is quite different: the gas temperature falls very little away from the peak.

If the gas and dust are thermally coupled, the relative variations of T_d and T_g find a natural explanation in a changing volume density. This is discussed more fully in § IIId.

c) The Column Density of Dust and Gas

The emission optical depth of dust at 118 μm, τ_{118}, was mapped in S201, and the results are presented in Fig. 3. It shows a sharp peak at the position of strongest far-infrared and the radio continuum emission, and the probable location of the exciting star(s). Such a coincidence is common, although not always the case, in objects like S201.

The optical depth appears to form an east-west ridge in Fig. 3, with τ_{118} falling fairly sharply to the north and south. Much the same effect is seen by Martin and Barrett (1978) in their calculated CO column density: the mass structure of S201 is dominated by an east-west, high column density ridge. One qualitative difference between the CO results and those for the dust is the fairly abrupt drop in τ_{118} an arcminute or two east of the maximum. The CO shows no such sharp drop at this point and it might be an effect due to emission in the reference beam, as noted in § IIIa. At other positions in Fig. 1, the reference beam was in a position of low gas temperature and/or column density. We believe that the other points were therefore uncontaminated.

The relationship between CO column density, N(CO), and dust emission optical depth is an important quantity in a number of studies of star-forming regions. With the map of CO column density of Martin and Barrett, a point-by-point comparison with τ_{118} can be made. This is particularly interesting with S201, where the calculated dust optical

depth varies by nearly a factor of 40 within the same object (Fig. 3) and the beam sizes of the observations were similar. Fourteen points in the source were observed in common between ourselves and Martin and Barrett. A plot of $N(^{13}CO)$ from their data vs. τ_{118} at the same position is presented in Fig. 4. The relationship between A_V and $N(^{13}CO)$ found by Dickman (1978) for fairly low column density clouds was used to calculate the equivalent extinction, shown on the right axis. Generous factor-of-two error bars for τ_{118} are included. Because of these fairly large uncertainties in τ_{118}, it is of little use to try to derive a relation between $N(^{13}CO)$ and τ_{118} from our data. Instead, we wish to see how well our data fit such relations derived by other workers.

The shaded sector in the figure is the range of the relations between the 85 μm emission optical depth and $N(^{13}CO)$ found by Sargent et al. (1981) in four star-forming regions. For Fig. 4, the 85 μm optical depth was corrected to that at 118 μm by assuming an absorption coefficient that varied as λ^{-1}. As the figure clearly shows, there is quite reasonable agreement between our results and those of Sargent et al. for $\tau_{118} = 3 \times 10^{-19} N(^{13}CO) = 8 \times 10^{-4} A_V$, the average of the shaded region. This value is in some disagreement with $\tau_{350} = 6 \times 10^{-19} N(^{13}CO)$ found by Righini-Cohen and Simon (1977). This is probably due in part to the necessity of assuming dust temperatures in the Righini-Cohen and Simon work, some of which were poor approximations to the subsequently measured values. Figure 4 probably is in good agreement with that found by Evans, Blair, and Beckwith (1977), who estimated a flux-weighted-mean far-infrared optical depth to have $\tau_{FIR} \approx 10^{-18} N(^{13}CO)$. Although the maximum flux density in S201 (and many

other similar objects) is near 90 μm, most of the flux is emitted between 20 μm and 60 μm. Therefore, the average far-infrared optical depth of Evans, Blair, and Beckwith properly applies to wavelengths around 40 μm. For a λ^{-1} dependence of the absorption coefficient then, the τ-to-N(^{13}CO) relation they found is in good agreement with ours and that of Sargent et al. (1981).

Despite the large uncertainty in τ_{118}, there is an interesting effect in Fig. 4 that is probably real. At values of N(^{13}CO) below about 5 x 10^{15} cm^{-2} ($A_V \leq$ 2 mag), the observed τ_{118}/N(^{13}CO) ratio increases significantly over the average value. This is just what is expected if a minimum amount of dust is necessary to protect the CO from photo-destruction (e.g., Liszt 1978, Glassgold and Langer 1976, and references therein). For N(^{13}CO) $\gtrsim$ 7 x 10^{15}cm^{-2} ($A_V \gtrsim$ 3), the observed points — with their large uncertainties — seem to follow the average, shaded relation in Fig. 4 very well.

It is probably worth noting that for sources with a much higher column density (N(^{13}CO) $\gtrsim$ 10^{17} cm^{-2}) or far-infrared emission optical depth ($\tau_{FIR} \gtrsim$ 0.1), the relationship found by Sargent et al., and shown in Fig. 4, gives poor agreement (cf., Werner et al. 1980; Thronson et al. 1978; Thronson and Harper 1979). On the other hand the very different relation found by Righini-Cohen and Simon that fit poorly in Fig. 4 gives somewhat better agreement. This type of effect might be expected as a result of the method of calculating T_d (§ II). The fundamental assumption is that the object is isothermal, an approximation that is more likely fulfilled in the more optically-thin sources (like S201) than in those that are more opaque. In the latter case, a step gradient in T_d exists, making an estimate using a single

temperature highly uncertain. If there is a constant gas-to-dust ratio among molecular sources, it is therefore probably more accurately determined in objects like S201 where the necessary approximations do not lead to large errors.

d) The Volume Density Structure

The previous section discussed the dust and gas column density in the source. With the extensive data available on S201, we may use the assumption of dust-to-gas thermal coupling to estimate volume densities for the region in the source that dominates the far-infrared emission. This knowledge is desirable because of the fundamental role that the density plays in determining cloud structure and evolution. In addition, the method described below offers an alternative — and we believe acceptably accurate — method to the use of radio molecular observations. Our technique does not suffer from major optical depth effects, or from the consequences of unusual excitation that can complicate the radio techniques, although this method has several uncertainties of its own.

It is assumed that the dominant heat source for the molecular cloud is embedded stars, and that the gas is heated only by collisions with the dust. This mechanism has been discussed theoretically by a number of authors (e.g., Goldreich and Kwan 1974; Goldsmith and Langer 1978; Ho, Martin, and Barrett 1981). The largest internal uncertainties in the method adopted here are in the calculation of dust temperatures (§ II) and some grain parameters. Fortunately, these uncertain values enter linearly (or weaker) into the calculations, rather than exponentially or to some high power. Probably the most significant external uncertainty is the implied coexistence of the gas and dust seen in emission: this paper, like most others of its type, assumes that the region that dominates the far-infrared emission also is the source of CO emission. It is beyond the scope of this paper to address this question fully.

Our approach is to infer the grain parameters at one point in the cloud, and then use this set over the whole region to find the local density. Consider the rate of energy transfer between gas and dust:

$$\Lambda_{gd} = 5.3 \times 10^{-36} \left(\frac{f\xi}{a\rho}\right) n_{H_2}^2 T_g^{\frac{1}{2}} \Delta T \text{ ergs cm}^{-3} \text{ s}^{-1}$$

adapted from Leung (1975). Here the uncertain grain parameters are all placed in parentheses in the equation: f is the dust-to-gas mass ratio ($\sim$0.01), ξ is the grain accomodation coefficient ($\sim$0.6), a is the grain radius ($\sim$0.1μm), and ρ is its specific density ($\sim$ 2 gm cm^{-3}). These numerical values are commonly suggested for the parameters. In the equation, T_g is the gas temperature (assumed to be equal to the CO excitation temperature) and ΔT is the observed difference between the gas and dust temperatures. This energy input rate is equated with the total gas cooling rate tabulated in Goldsmith and Langer (1978), which depends only upon T_g and n_{H_2}. Therefore, the molecular hydrogen density can, in theory, be directly determined from observed quantities. The largest uncertainty in the calculation is for the parenthetical value in the equation above. Rather than adopt the nominal values for each parameter, giving $(f\,\xi/a\rho) \tilde{\sim} 250$, we normalize this ratio to that at one position in S201.

We take the far-infrared peak as the point for this normalization. Martin and Barrett (1978) estimated a lower limit of $n_{H_2} \geq 4 \times 10^3$ cm^{-3} from analysis of CS line emission from this position. Alternatively, we can use their CO column density, a relative abundance of $[CO]/[H_2] = 5 \times 10^{-5}$, and a characteristic source size equal to the north-south dimension of the S201 molecular cloud (2 pc), to find $n_{H_2} = 6 \times 10^3$

cm^{-3}. Because CO can be excited by densities along the line of sight as low as a few times 10^2, this value is probably also a lower limit. For this reason, we take $n_{H_2} = 10^4$ cm^{-3} at the peak. It unlikely to be much greater at the center of S201, otherwise Martin and Barrett should have detected NH_3 emission. The local density certainly must be less than 10^5 cm^{-3}, since at these large values the Goldsmith and Langer models predict that $T_d \approx T_g$. To a good approximation, densities calculated at other positions vary linearly with the adopted peak density. Thus the relative values over the source are fairly firm, even if the absolute values probably are uncertain to at least a factor of 5.

The same points used to compare τ_{118} and $N(^{13}CO)$ in the previous section were used to find n_{H_2} using the method described above. We find the distribution of volume density is qualitatively similar to that of CO column density or infrared optical depth (Fig. 3). That gives us confidence that our calculated n_{H_2} is measuring a real effect in S201. The density falls off in all directions away from the peak, though by no means as fast as τ_{118} in Figure 3. To the north and south, $n_{H_2} = 2 - 5 \times 10^3$ cm^{-3} one and two arcminutes from the peak. Directly west, however, the density equals 5×10^3, 8×10^3, and 15×10^3 cm^{-3} in steps of 1, 2, and 3 arcminutes. In the area mapped in the far-infrared, then, the highest volume density appears significantly offset from the exciting star(s). Of course, the density could rise higher even further to the west, beyond the extent of the infrared map. This is in the direction of the highest T_g in the region (Martin and Barrett), and certainly an area for further study in the infrared. We should repeat that these calculated densities properly apply only to the region of the source emitting in the far-infrared, probably the more central parts of the cloud.

It is worth noting the effects of uncertainties on the results. It was noted above that the dust parameters might be found at one position in an object, as was done for S201, and with some confidence assumed to be constant throughout. In the case of S201, the internal errors of measurement of T_d and T_g — the other input parameters for the method — are typically less than ±2 K and have virtually no effect on n_{H_2}. The external, systematic errors are more significant. If T_d has a total uncertainty of ± 25% ($\sim$± 10K) and T_g can be correctly estimated to ±15% ($\sim$±3 K), in S201 the typical absolute uncertainty in n_{H_2} will be about a factor of two (note again that the relative values will be more accurate). This error in n_{H_2} is due in about equal parts to the large possible errors in T_d, and to the fairly sensitive dependence of n_{H_2} on T_g in this method (see Goldsmith and Langer). We note that these uncertainties estimated for T_d and T_g are probably significantly larger than in actual practice. If it should happen that there are other sources of gas-heating besides the warm dust in our object, n_{H_2} would be an upper limit.

e) The Grain Size in S201

In the previous section a value for the ratio of four important grain parameters, $(f\xi/a\rho)$, was found at the infrared peak of S201. If $n_{H_2} \leq 10^4$ cm^{-3} at this position, as discussed above, $(f\xi/a\rho) \leq 700$ cm^2 gm^{-1} if the gas is heated only by the dust. This allows a limit to be placed on grain size. Cosmic abundances put a very strong limit on the dust-to-gas mass ratio, $f \leq 0.02$, and the accommodation coefficient, ξ, by definition cannot be larger than 1. Therefore we have $a\rho \leq 2.9 \times 10^{-5}$ gm cm^{-2}. Since the specific grain density, ρ, is unlikely to be less than 2 gm cm^{-3}, we find $a \leq 0.15$ μm for a mean

grain radius in S201. Since all the limits used in this calculation, with the possible exception of ρ , were very strong, the upper limit to the radius probably can be lowered by at least a factor of two. The typical far-infrared-emitting grain in S201 therefore appears very similar in size to that found in the "standard" interstellar medium, and there is no evidence here for the very large grains sometimes suggested to be found in regions like S201.

It is worth noting here that although a fairly low limit was calculated for only S201, the result can be generalized to almost every star-forming region so far observed. The fact that high gas temperatures (T_g = 20-60 K) and high densities ($n_{H_2} = 10^3$-10^5 cm^{-3}) commonly characterizes the clouds surrounding the young stars means that grains sizes cannot be large. This can be seen by equating the rate of energy transfer, Λ_{gd} above, with the high-density cooling rate of Goldsmith and Langer. Using the limiting values for grain parameters, one gets $a(\mu m) \leq 3.5\ T_g^{-2.2}\Delta T$ for $n_{H_2} = 10^4$ cm^{-3}. Since the difference between the gas and dust temperatures, ΔT, rarely exceeds $\sim$ 20K, the grain radius is always going to be a small fraction of a micrometer. This result simply reflects the apparent fact that at, or above, moderate densities the cooling rate is both large and a strong function of T_g. The heating rate per cubic centimeter of the gas depends upon a factor that includes the volume density of the grains multiplied by the grain surface area. For a constant gas-to-dust mass ratio, this factor depends inversely upon grain diameter. Therefore, to a rough approximation, radio molecular observations of high gas temperatures naturally implies modest grain sizes.

IV. SUMMARY

The results of our study of S201 can be summarized in the following statements.

1. The total luminosity measured in the source is 5.2 ± 1.3 X $10^4 L_\odot$, equivalent to an O9 ZAMS star and in good agreement with that deduced from radio continuum measurements. The entire molecular cloud was not mapped and there may be significant infrared emission from the other CO hotspot in the cloud.

2. The dust temperature distribution is consistent with heating by a centrally-located embedded object.

3. The dust emission optical depth shows a distribution qualitatively similar to that of ^{13}CO. A τ_{118}-to-N(^{13}CO) plot was found to be in good agreement with work by some other observers. Our relation did not, however, agree with that estimated for more optically thick objects. The edges of S201 seem to show the effects of enhanced CO destruction, possibly due to lack of protection by the dust.

4. The assumption that the molecular gas is heated via collisions with the dust allows a direct calculation of the particle density. The results are in fairly good agreement with those determined from the radio molecular results. The far-infrared peak has high volume densities, but not as high as positions further west, in the direction of the brightest radio molecular hotspot.

5. The assumption of gas-dust coupling in the heating also allowed a strong upper limit to be placed on the radius of the infrared-emitting grains, $a \leq 0.15$ μm. The general question of grain sizes in hot-centered star-forming clouds was discussed.

ACKNOWLEDGEMENTS

We are grateful to the crew of the Kuiper Airborne Observatory for continued excellent support. This work was supported by NASA grant NAG 2-134.

REFERENCES

Evans, N. J., Blair, G. N., and Beckwith, S. 1977, Ap. J., 217, 448.

Dickman, R. L., 1978, Ap. J. Suppl. 37, 407.

Gehrz, R. D., Hackwell, J. A., and Jones, T. W. 1974, Ap.J., 191, 675.

Georgelin, Y. M., and Georgelin, Y. P. 1976, Astr. Ap., 49, 57.

Glassgold, A. E., and Langer, W. D. 1976, Ap. J., 206, 85.

Goldreich, P., and Kwan, J. 1974, Ap. J., 189, 441.

Goldsmith, P. F., and Langer, W. D. 1978, Ap. J., 222, 881.

Ho., P. T., Martin, R. N., and Barrett, A. H. 1981, Ap. J., 246, 761.

Kleinmann, S. G., Joyce, R. R., Sargent, D. G., Gillett, F. C., and Telesco, C. M., 1979. Ap. J., 227, 126.

Lada, C. J., Thronson, H. A., Smith, H. A., Harper, D. A., Keene, J., Loewenstein, R. F., and Smith, J. 1981, Ap.J. (Letters), 251, L91.

Lada, C. J., Elmegreen, B. G., Cong, H., and Thaddeus, P. 1978, Ap. J. (Letters), 226, L39.

Leung, C. M. 1975, Ap. J., 199, 340.

Leung, C. M. 1976, Ap. J., 209, 75.

Liszt, H. S. 1978, Ap.J., 22, 484.

Martin, R. N., and Barrett, A. H. 1978, Ap. J. Suppl, 36, 1.

Righini-Cohen, G., and Simon, M. 1977, Ap. J., 213, 390.

Rowan-Robinson, M. 1980, Ap. J. Suppl., 44, 403.

Sargent, A. I., van Duinen, R. J., Fridlund, C. V., Nordh, H. L., and Aalders, J. W. 1981, Ap. J., 249, 607.

Schwartz, P. et al. 1983, Ap.J., 271 in press.

Scoville, N. Z., and Kwan, J. 1976, Ap. J., 206, 718.

Smith, H. A., Thronson, H. A. Lada, C. J., Harper, D. A., Loewenstein, R. F., and Smith, J. 1982, Ap. J., 258, 170.

Thronson, H. A. Harper, D. A., Keene, J., Loewenstein, R. F., Moseley, S. H., and Telesco, C. M. 1978, A. J., 83 492.

Thronson, H. A., Lada, C. J., Harvey, P. M., and Werner, M. W. 1982, M.N.R.A.S., 201, 429.

Thronson, H. A., and Price, S. 1982, A. J., 87, 1288.

Vallee, J. P., Hughes, V. A., and Viner, M. R. 1979, Astr. Ap., 80, 186.

Werner, M. W. et al. 1980, Ap. J., 242, 601.

TABLE 1

Source Parameters

Peak Position (Far-infrared)	$\alpha(1950) = 2^h\ 59^m\ 21\overset{s}{.}4 \pm 2^s$ $\delta(1950) = 60°\ 16'\ 15'' \pm 15''$
Total flux density	
11 μm[a]	40 Jy
20 μm[a]	100 Jy
62 μm[b]	2600 Jy
118 μm[b]	4000 Jy
Peak flux density	
2.3 μm	0.066 ± 0.028 Jy
4.9 μm	0.062 ± 0.024 Jy
10 μm	0.55 ± 0.08 Jy
19.5 μm	0.77 ± 0.15 Jy
Far-infrared luminosity	$5.7 \times 10^4\ L_\odot$ (09 ZAMS)
Dust temperature at the peak	42 ± 2[c] K
115 μm optical depth at the peak	0.011[d]

[a] Thronson and Price (1982); estimated total uncertainty ± 50%.

[b] This work; estimated total uncertainty ± 25%

[c] Range allowed by internal uncertainties only. Total uncertainties ± 5K.

[d] Estimated ± 50% internal uncertainty.

contours are logarithmic: each is a factor of two larger than the next lower one. The peak value is $\tau_{118} = 0.011$.

Figure 4. A plot of the 118 μm emission optical depth, found for Figure 2, versus the ^{13}CO column density from Martin and Barrett (1978). Shown in the cross-hatched region is the range of relationships between CO and τ_{85} found by Sargent et al. (1981). The horizontal bars on each point show the factor-of-two uncertainty estimated for τ. The relation between $N(^{13}CO)$ and A_V found by Dickman (1978) was used to normalize the right axis.

FIGURE CAPTIONS

Figure 1. The flux density distribution in S201. Figure 1a is from the 45-80 μm bandpass filter and Figure 1b is from the $\lambda \geq 85$ μm system. As noted in the text, the dust temperature varies so little over the source that the effective wavelength of the broadband filter varies by no more than ± 10% of the value in the figure. The contour levels are at 0.05, 0.1, 0.2, 0.4, 0.6, and 0.8 of the peak. The dashed lines are extrapolations. The 62 μm map is normalized so 1.00 ≡ 710 Jy and the 118 μm has 1.00 ≡ 845 Jy. A typical 1σ internal uncertainty is 0.02 of the peak, although at the outer coutours the uncertainty is closer to 0.01. The extent of the mapping was one-half beamwidth beyond the lowest contour, on average.

Figure 2. The spectrum of the S201 region. The small solid dots are the values measured in a 49" beam at the peak. The open circle is a value measured in a 128" beam. The large solid dots are total flux densities for the source (Table I). The solid line is a curve of the form $\nu B_\nu(T)$ fit to only the 62 μm and 118 μm points. For the peak position, T = 42 K. The error bars are an estimated ± 20% total uncertainty.

Figure 3. The distribution of 118 μm emission optical depth in units of 10^{-3}. It was found assuming that $F_\nu = \tau_{118} B_\nu(T_d)\,\Omega$, where Ω is the beam solid angle. The internal uncertainty is estimated to be ± 50%; the values are probably accurate to a factor two. Note that the

ADDRESSES

W. Glaccum, D. A. Harper, R. F. Loewenstein, and J. Smith
Yerkes Observatory, Williams Bay, WI 53191

C. J. Lada
Steward Observatory, University of Arizona, Tucson, AZ 85721

H. A. Smith
Space Science Division, Naval Research Lab, Washington, DC 20375

H. A. Thronson, Jr.
Department of Physics and Astronomy, University of Wyoming,
Laramie, WY 82071

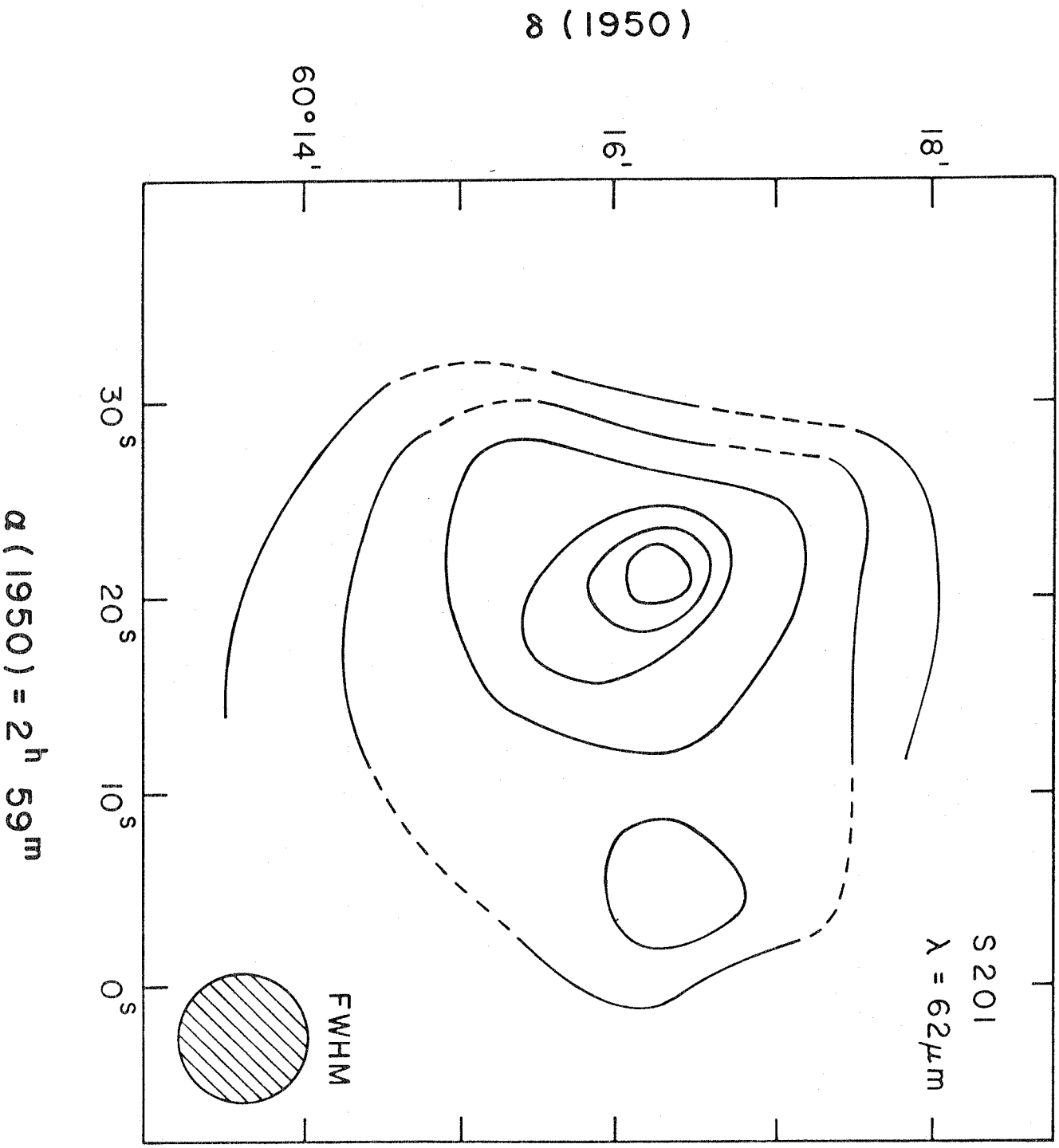

Fig. 1a

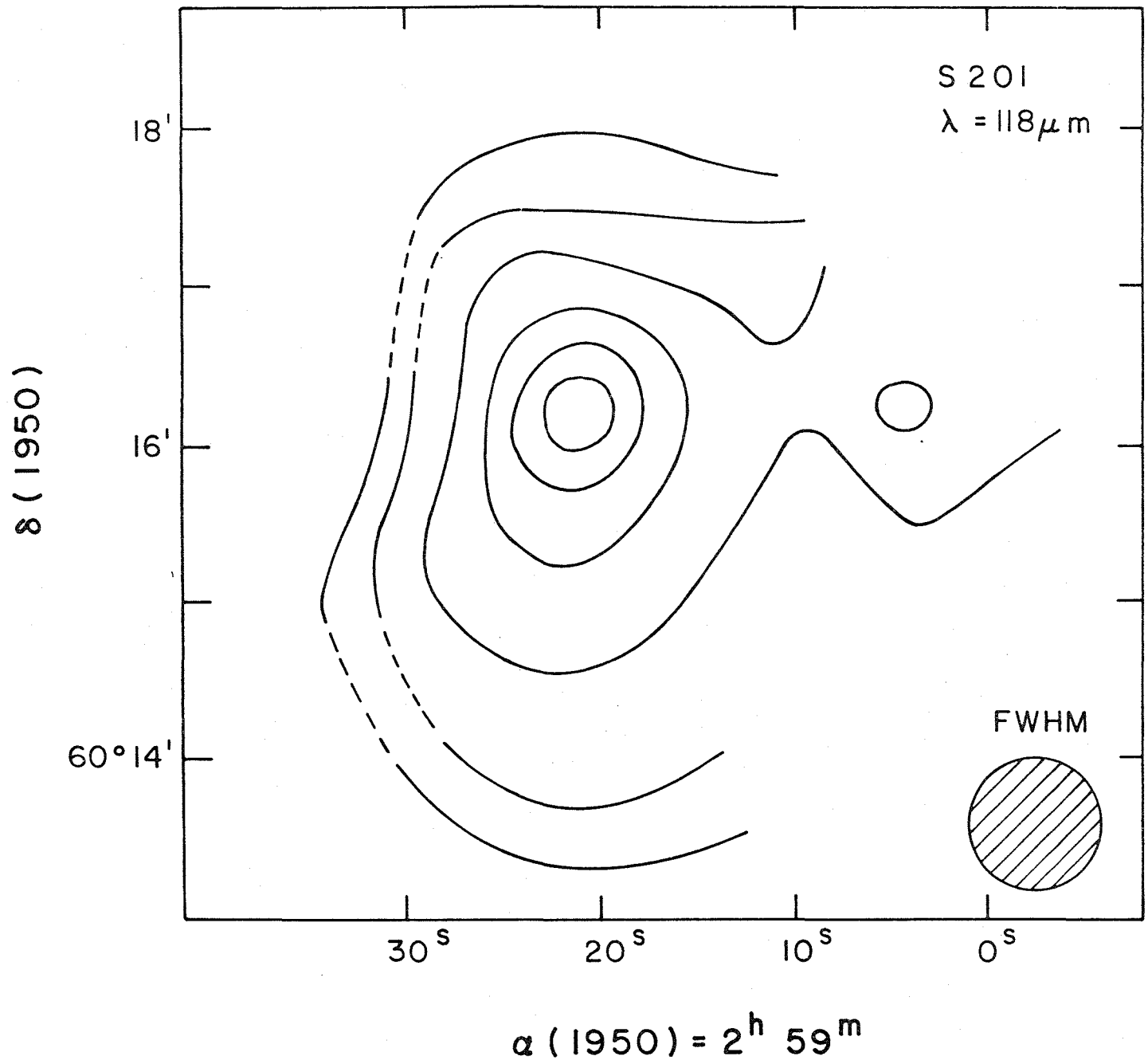

Fig. 1b

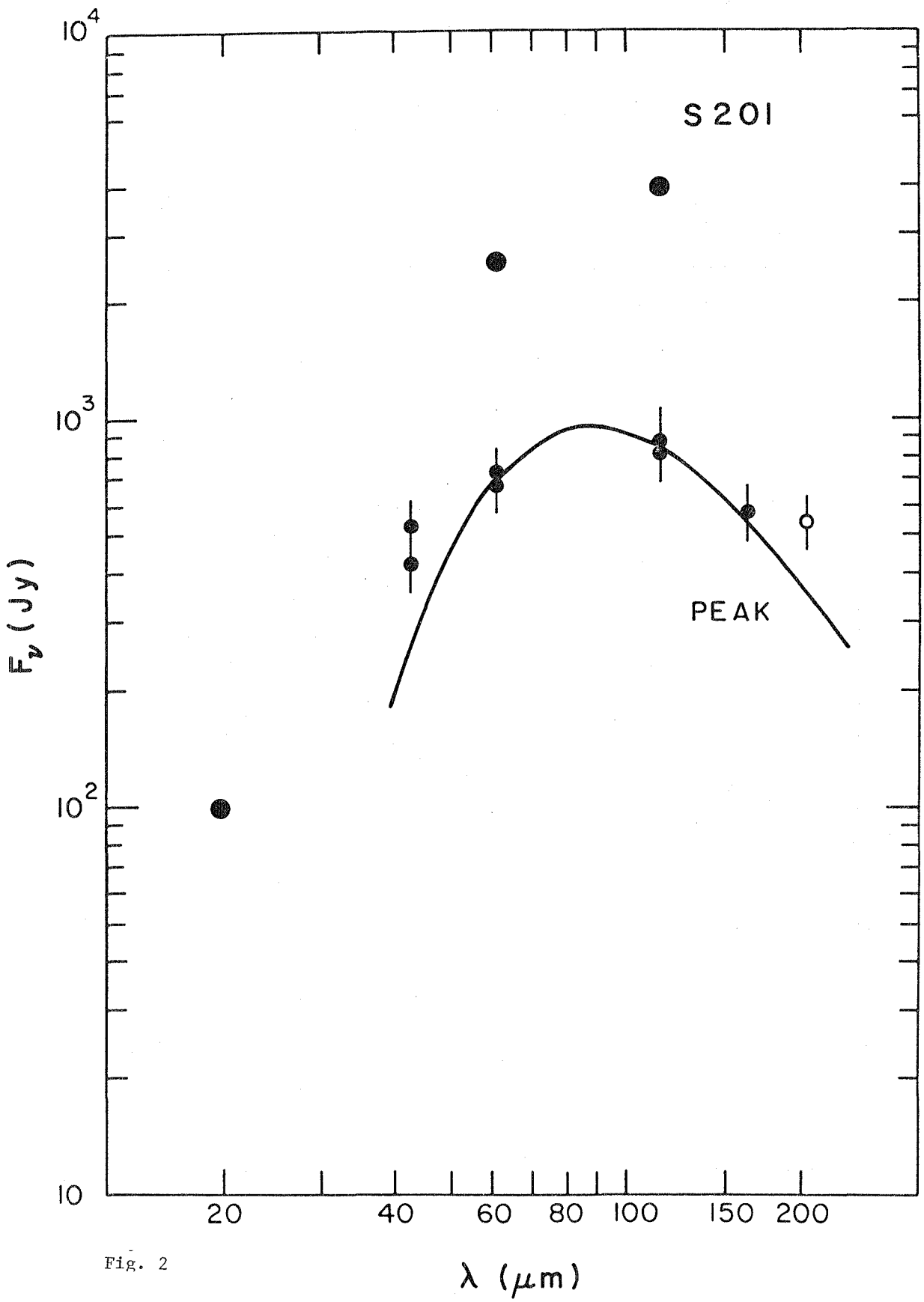

Fig. 2

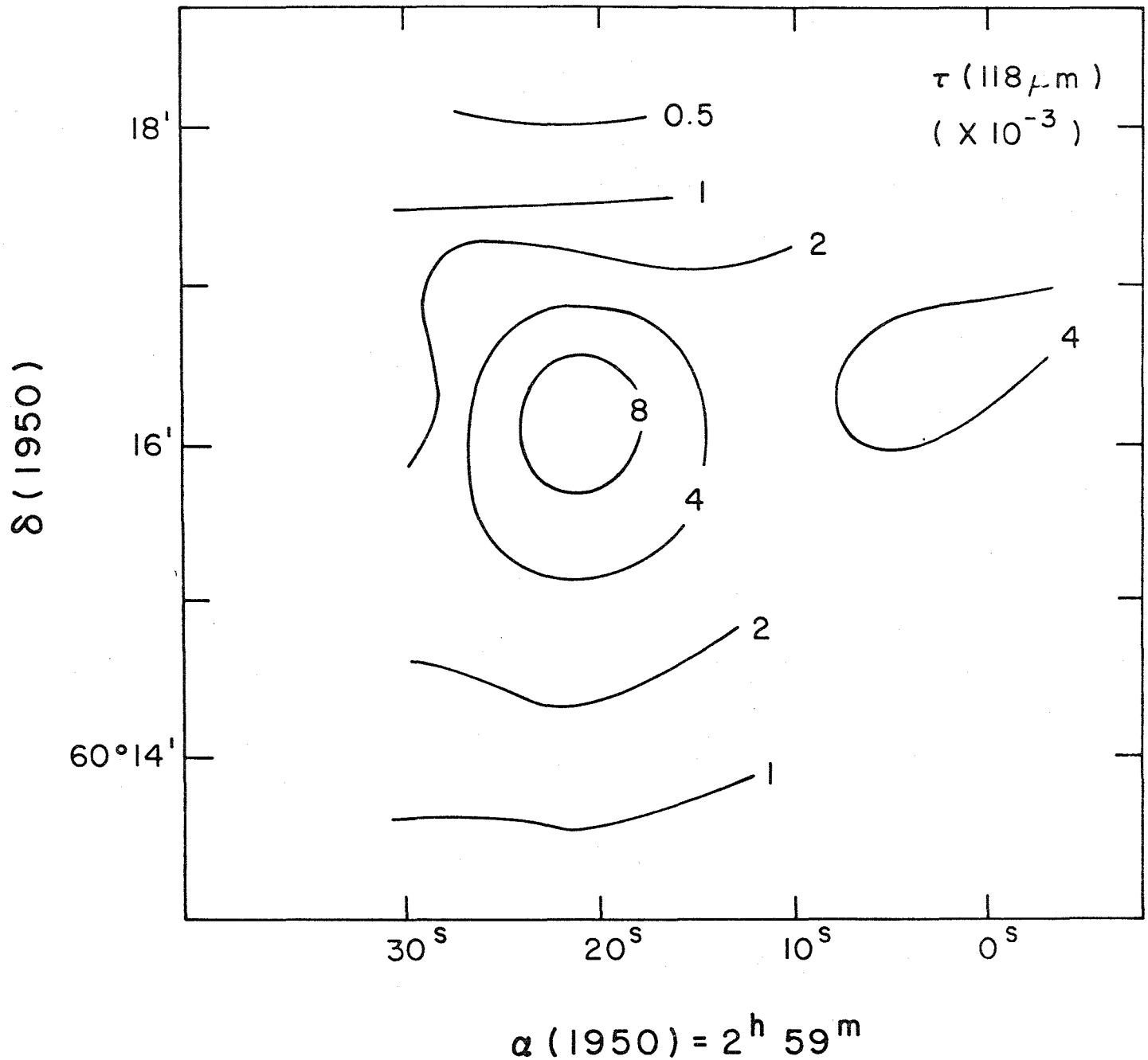
τ (118 μm)
(X 10⁻³)
0.5
1
2
4
8
4
2
1
18'
16'
60°14'
δ (1950)
30 s
20 s
10 s
0 s
α (1950) = 2h 59m

Fig. 3

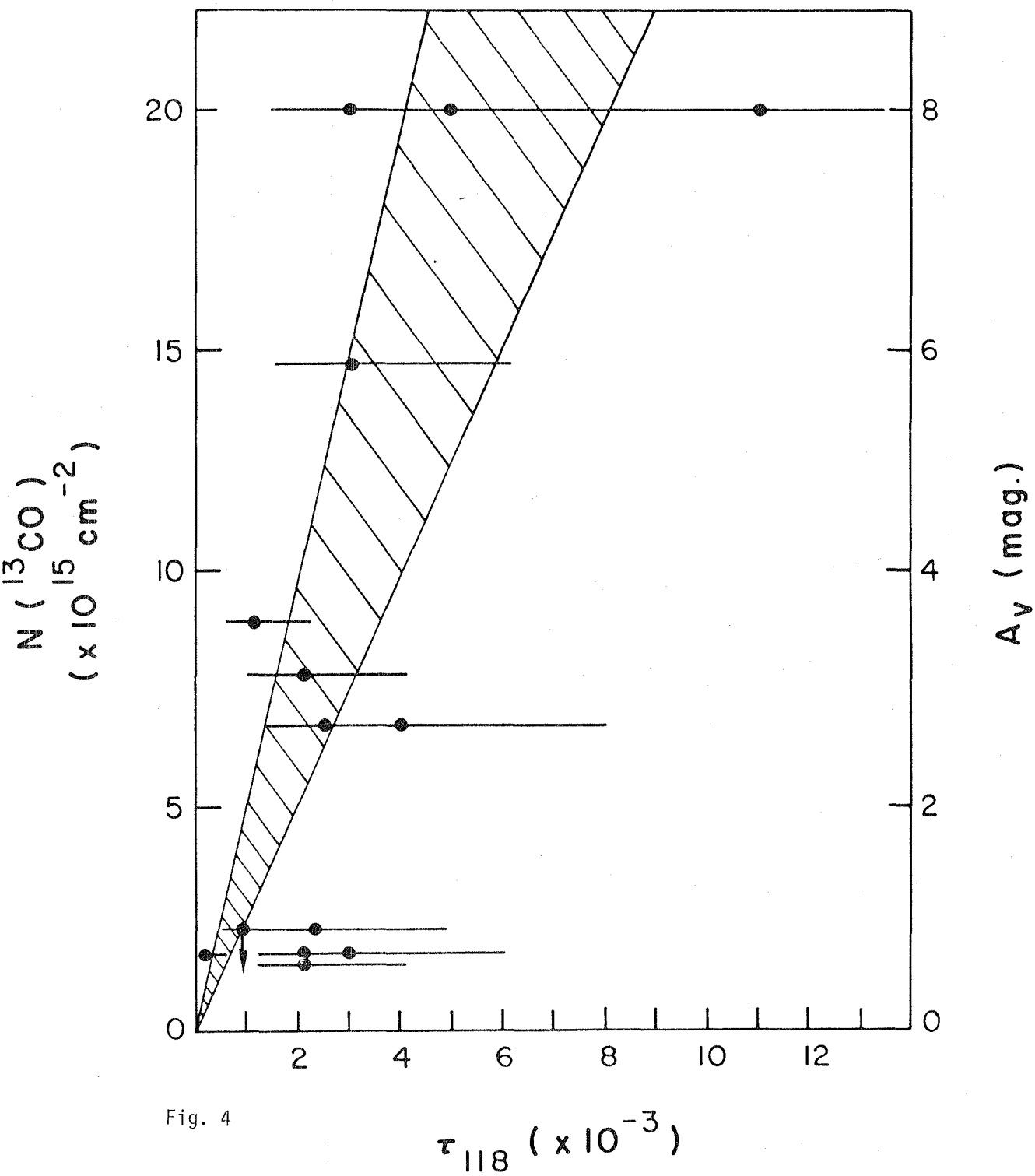

Fig. 4

1. Report No.	2. Government Accession No.	3. Recipient's Catalog No.
NASA TM-85953		

4. Title and Subtitle	5. Report Date
THE ENERGETICS AND MASS STRUCTURE OF REGIONS OF STAR FORMATION	May 1984
	6. Performing Organization Code A-9738

7. Author(s)	8. Performing Organization Report No.
Harley A. Thronson, Jr.,* Howard A. Smith,† Charles J. Lada,† W. Glaccum,§ D. A. Harper,§ R. F. Loewenstein,§ and J. Smith§	A-9738
	10. Work Unit No. T-5726

9. Performing Organization Name and Address	11. Contract or Grant No.
*Wyoming Infrared Observatory, Univ. of Wyoming, Laramie, WY 82071 †E. O. Hulburt Center for Space Research, Naval Research Laboratory, Washington, DC 20375 †Steward Observatory, Univ. of Arizona, Tucson, AZ 53191 §Yerkes Observatory, Univ. of Chicago, Williams Bay, WI 53191	

12. Sponsoring Agency Name and Address	13. Type of Report and Period Covered
National Aeronautics and Space Administration Washington, DC 20546	Technical Memorandum
	14. Sponsoring Agency Code 352-02-03

15. Supplementary Notes

Preprint Series #012. Supported by NASA grants.
Point of Contact: L. C. Haughney, Ames Research Center, M.S. 211-12, Moffett Field, CA 94035
(415) 965-5339 or FTS 448-5339

16. Abstract

A number of theoretical predictions about dust and gas in star-forming regions are tested by observing a 4' region surrounding the radio continuum source in S201. The object was mapped in two far-infrared wavelengths and was found to show significant extended emission. Under the assumption that the molecular gas is heated solely via thermal coupling with the dust, the volume density was mapped in S201. The ratio of infrared optical depth to CO column density was calculated for a number of positions in the source. Near the center of the cloud our values are found to be in good agreement with other determinations for lower column density regions. In addition, our observations suggest significant molecular destruction in the outer parts of the object. Current models of gas heating were used to calculate a strong limit for the radius of the far-infrared-emitting grains, $a \leq 0.15$ μm. In addition, we argue that grains of about this size are required by the observation of high-temperature ($T \geq 20$ K) gas in many sources.

17. Key Words (Suggested by Author(s))	18. Distribution Statement
Infrared: Sources Interstellar: Dust and molecular gas Stars: Formation	Unlimited Subject Category - 89

19. Security Classif. (of this report)	20. Security Classif. (of this page)	21. No. of Pages	22. Price*
Unclassified	Unclassified	33	A03

*For sale by the National Technical Information Service, Springfield, Virginia 22161

End of Document